Optica Applicata, Vol. XXXI, No. 3, 2001

Application of automated interferometric system for investigation of the behaviour of a laser-produced plasma in strong external magnetic fields

ANDRZEJ KASPERCZUK, TADEUSZ PISARCZYK

Institute of Plasma Physics and Laser Microfusion, ul. Hery 23, 00–908 Warszawa 49, Poland.

In this paper, achievements of the authors in the field of technical and numerical problems of multi-frame interferometry are presented. A three-channel interferometric system with an automatic image processing for laser-produced plasma is described. The measurements of electron density distributions in a plasma generated by a laser and confined by a strong magnetic field (up to 15 T) are the main part of this work. Numerical analysis of interferograms of the plasma and numerical methods of the reconstruction of electron density spatial profiles both in an axially symmetrical plasma and in a plasma stream of disturbed axial symmetry are presented in more detail.

1. Introduction

The interferometry is a very important diagnostic tool in the investigations of a hot and high density plasma generated by a high power laser system. This diagnostic technique is a source of information about the dynamics and the space and time distribution of electron density in the plasma under investigation. Such rich experimental data allow us to draw many conclusions relating to the thermodynamic processes, a state of the magneto-hydro-dynamical equilibrium of the plasma, trapping of the plasma by a magnetic field and selection of an optimum configuration of the magnetic field from the point of view of different applications of the plasma, *etc.* Moreover, the interferometry is a comfortable instrument for the estimation of the laser beam distribution as well as quality of its focusing on the target.

In spite of the above unquestionable advantages the interferometric diagnostic method is rarely applied in plasma laboratories. The reasons for that are:

– complexity and high price of an interferometric diagnostic system,

– the necessity of possessing of indispensable software for the analysis and numerical treatment of interferometric pictures which would make it possible to shorten the process of determination of electron density distribution in the plasma investigated,

– competence and professional experience of scientific team required in the analysis of the interferograms as well as their knowledge in the field of the phenomena under investigation.

The authors of the present paper have all the facilities to realize a very interesting program of the investigation. The investigations of the influence of a strong external magnetic field of 5–20 T in induction on the dynamics and stability of a laser-produced plasma have recently been carried out in our laboratory. The plasma was produced from a flat teflon target by a Nd laser of energy 5–10 J and pulse duration roughly 1 ns. The studies were carried out both in axial and perpendicular geometries of the magnetic field lines corresponding to the direction of the laser beam. It should be pointed out that the majority of work on this subject concerns the interaction of plasma with a relatively weak magnetic field ($B_0 < 1$ T). Up to now, articles concerning the interaction of plasma with a magnetic field ranging from 5 to 15 T were very scarce.

In the paper there are presented achievements of the authors, including: an automated system for registration and analysis of interferometric pictures, methods of numerical reconstruction of electron density spatial profiles both in symmetrical and asymmetrical plasma as well as selected aspects of the investigation of laser-produced plasma in a strong external magnetic field.

2. Automated three-channel interferometric system for measuring the electron density distribution in a laser-produced plasma

2.1. Acquisition system of interferograms

Among many experimental methods of the electron density determination in a plasma the most reliable and useful one is the interferometry. In the case of an axially symmetrical plasma a laser beam with an aperture larger than the dimensions of the plasma is used for illumination of the interferometer. This diagnostic method enables us to obtain information about space and time electron density distribution of a laser -produced plasma. The space distributions of the electron density are determined (with the use of the Abel transformation [1]) on the basis of the two-dimensional phase distributions of the radiation probing the plasma. The phase distributions are determined based on the displacement of the fringes which appear in the interferometric image. The correct reproduction of the phase distribution in a plasma is a very difficult and time-consuming task which also requires professional experience.

Figure 1 presents a block diagram of a three-channel automated interferometric system [2] which enables both space and time resolved measurements to be carried out. This system was constructed at the Institute of Plasma Physics and Laser Microfusion within the research project No. 8 8084 91/p02 granted by the Scientific Research Committee of the Polish Government (KBN).

Each of the interferometric channels is equipped with a miniature interferometer [3], [4] (of the folding wave type) which is illuminated by one of the Nd laser harmonics. The beam used for illumination was created as a part of the main laser beam. An optical scheme and principle of operation of the interferometer is presented in Fig. 2. Interferometric image in this interferometer is obtained by the separation,

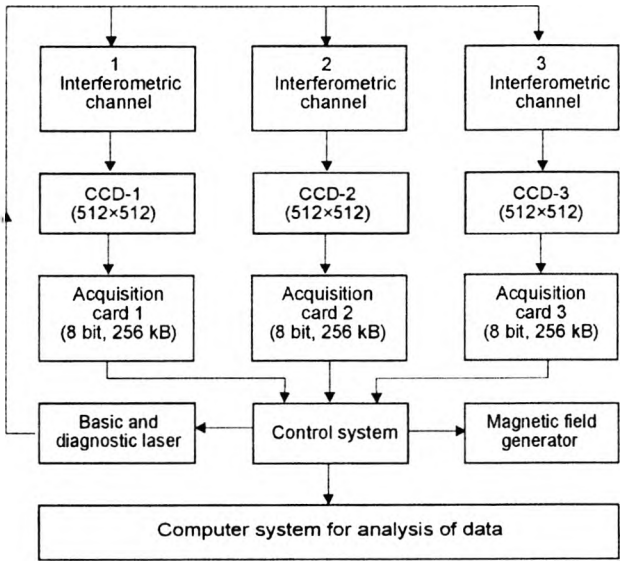

Fig. 1. Schematic block of the three-channel automated interferometric system for investigation of a laser -produced plasma.

inversion, and folding of the front face of a probing wave. According to the principle of operation of this interferometer the diameter of a probing beam should be at least twice that of the plasma. Analysing the optical scheme of the interferometer one can derive the following formulas for describing the width of interference fringe Δd, and the distance between the object beam and the reference beam, in the registration plane d [4]:

$$\Delta d = \frac{(b-f)\lambda}{2nf\gamma}, \tag{1}$$

$$d = \frac{1}{2}\left[b-\left(\frac{b}{f}-1\right)L\right]n\gamma \tag{2}$$

where: γ – refraction angle of wedge, λ – wavelength of the probing radiation, n – refractive index, f – focal length of objective.

Using the above formulas, optimal conditions of the registration were determined. The interferometric measurements (which are presented in this paper) were carried out with the objective of the focal length f = 250 mm, the angle of the wedge $\gamma = 3°$ and magnification to about five. It enables us to obtain the required width of the interferometric fringes equal to about 40 μm in the registration plane of the interferogram.

Each of the recording interferometric channels is equipped with a CCD camera of the Pulnix TM-565 type, with the matrix of 512×512 pixels. Each camera has an

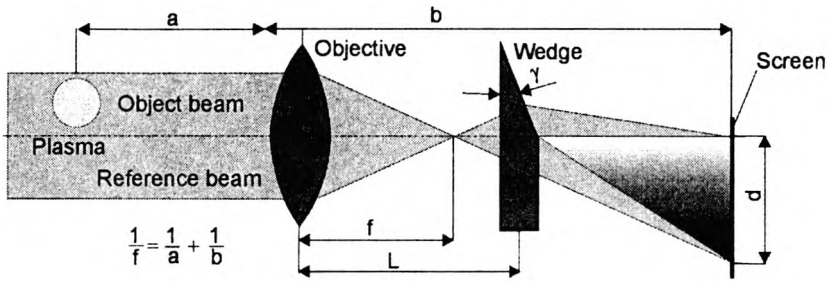

Fig. 2. Optical scheme and principle of operation of the interferometer.

assigned card of the analog-digital processing "frame grabber" type, with a resolution of 8-bits. Each camera channel operates independently and has its own buffer memory with a 256-kB capacity. The digitalized images from the cameras are retained in memory in their own acquisition channels. The images (512×512 pixels) retained in the memories can be displayed on TV monitors by means of 8-bit digital-analog converters.

The control system manages the work of each image acquisition channel and transfers the data to a computer. The control system enables synchronization of the recording system of three-channel interferometer with the laser generating the plasma (in the vacuum chamber) and with the magnetic field generator. To observe the phenomenon of interest in the plasma at the chosen time, the diagnostic beams (for each channel) were precisely synchronized by means of an optical delay line.

The picture acquisition system is controlled by using a special client-server application. It enables the process of picture acquisition to be controlled in the plasma experiment through the Internet from any software platform. Due to such a solution a remote control of the experiment is possible.

2.2. Computer processing of the interferograms

The methods which apply computer processing of the interferograms based on the fast Fourier transformation (FFT) algorithm [5]–[7] are an interesting alternative for the traditional methods relying on interpolation or approximation of the fringe distribution. The principlal advantage of the FFT methods lies in the possibility of automation of all the process of interferogram treatment [7]. This method is especially useful when the digital recording of the image by means of a CCD camera is applied. It enables us to determine the phase distribution directly on the basis of the digital interferometric image. In this manner one can avoid the arduous procedure of initial data processing connected with determination of the correct distribution of interferometric fringes. This procedure is very attractive but ineffective in the case of interferograms with the intensity varying considerably and the fringe distribution strongly disturbed. Such interferograms are usually registered in the investigation of the laser-produced plasma which is characterized by strong gradients of the electron density and temperature.

Unfortunately, the method based on the FFT is much complicated as regards the mathematical apparatus. The fundamental problem concerns the filtering of a space spectrum for the purpose of separation of the constant component (or reference fringes) and shifting "the information parts" of this spectrum to the beginning of coordinate system. In the case of illegible interferometric pictures the procedure of automatic searching for maxima in the space spectrum cannot be realized and then the reference point in this spectrum can be marked only by the manual intervention of an operator. Apart from the question of the filtering of the spectrum there are also problems connected with the cancellationng of the discontinuity appearing in the phase distribution. For this reason, the approximation of a phase distribution should be carried out but it is necessary to take into account that the error of the phase determination is then considerably amplified during the transition to the electron density distribution.

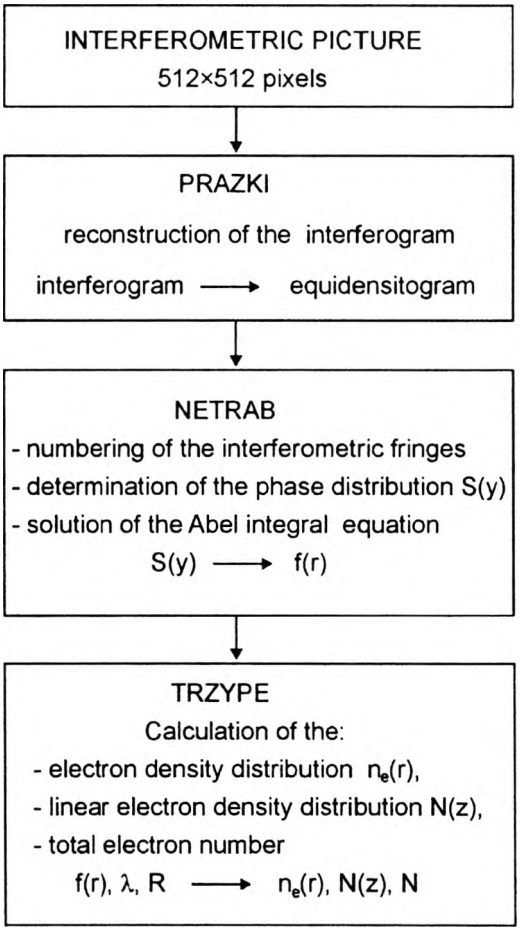

Fig. 3. Block diagram of a software for computer image processing.

The aforementioned inconveniences limit very strongly the application of the FFT method to the processing of complex interferograms of a plasma. This was confirmed in the papers which have been published up to now. In general, there are presented in the literature very simple examples of the processing of uncomplicated interferometric pictures, without more detailed information connected with the filtering of the space spectrum and reconstruction of the phase distribution.

Because of the above-mentioned difficulty the authors of this paper gave up the FFT method for treatment of the interferograms of a laser-produced plasma. For determination of the phase distribution on the basis of interferometric pictures there was applied the traditional method described below which is relatively simple and entirely credible. Taking into account that the precision of the determination of phase distribution depends only on the accuracy of the determination of the interferometric fringe position therefore the resolution of the CCD camera decides about the quality of the phase reconstruction (like in the case of the FFT method).

A special software has been prepared for the computational analysis of interferometric images [2] which enables reconstruction of the interferogram and then determination of the phase and electron density distributions in the laser-produced plasma. A block diagram which shows the succession of the computer processing of the interferogram is presented in Fig. 3.

The first step in the computer processing of the interferogram is to obtain equidense images with two levels of grey, namely, 0 and 256, where 0 corresponds to white fringes and 256 to the black ones. An example of the interferogram recorded in a laser -produced plasma experiment and the corresponding computer interferogram obtained by means of the PRAZKI program are shown in Fig. 4. The procedure producing an equidense image of fringes consist in that the cursor moves along the fringe, searching for its maximum or minimum for seven different directions containing the angle of

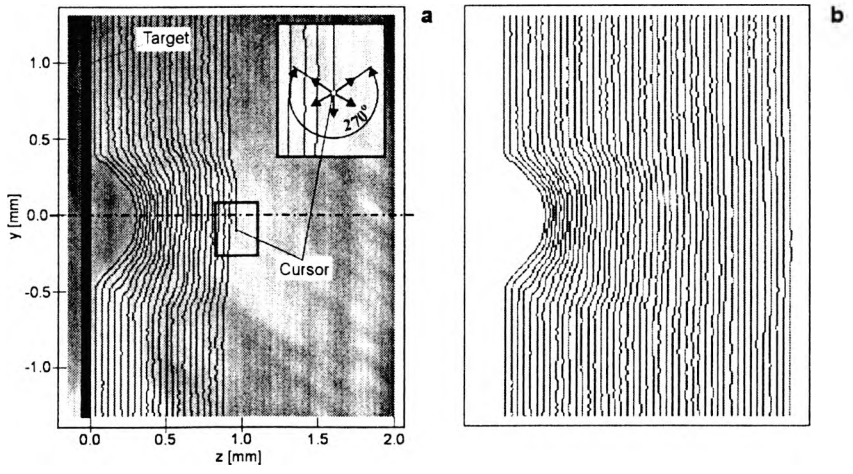

Fig. 4. Example interferogram of the laser-produced plasma registered by means of the CCD camera (**a**), and its computer reconstruction (**b**).

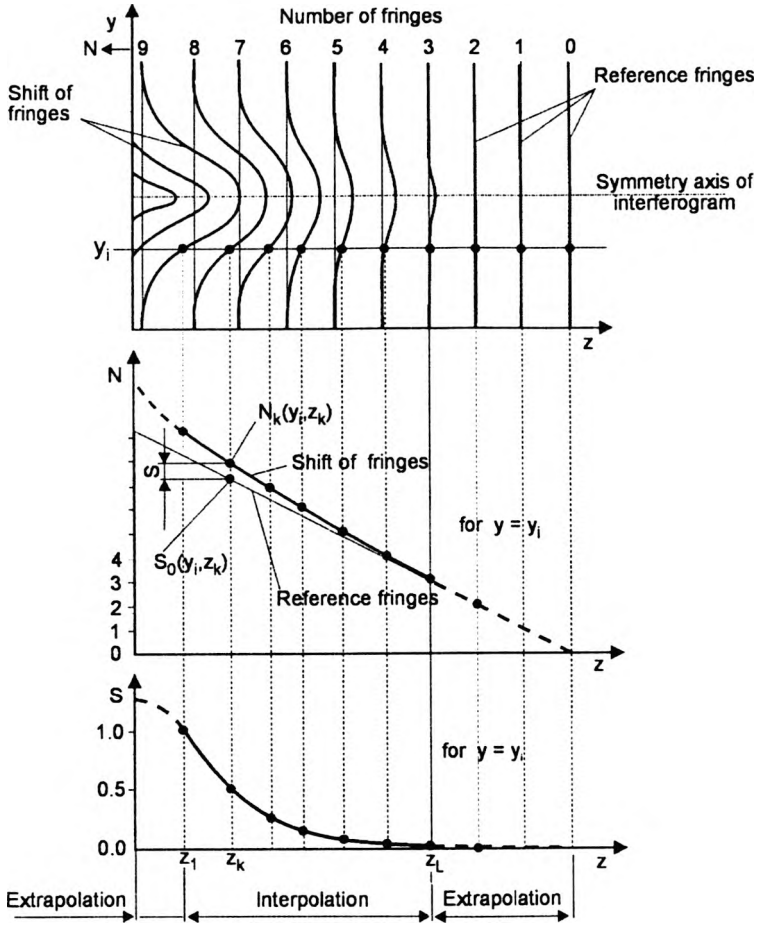

Fig. 5. Method of recovering the phase value from an interferogram.

270° (see Fig. 4**a**). Moreover, in the fragments of image where the fringes are blurred it is possible to reconstruct them by means of a cursor controlled from a keyboard or by a mouse.

The numbering of the fringes and determining from them the phase distribution is realized by the NETRAB program. All fringes are numbered starting from the chosen reference fringe (so-called zero-fringe), Fig. 5. For each fringe, there is assigned the set of points (y_i, z_i), describing its position in the coordinate system. Then, on the basis of distances between fringes and the position of the zero-fringes, the reference fringe system is built. It means that each fringe is assigned to its unshifted position. Knowing the position of shifted and unshifted fringes, a relation for all y_i = const between the absolute phase shift and the coordinate z is obtained

$$S = N_k(y_i, z_k) - S_0(y_i, z_k) = f(z_k)\big|_{y = y_i} \tag{3}$$

where: N_k is number of shifted k-th fringes at the point (y_i, z_i), and S_0 – the phase at the point (y_i, z_i), determined on the basis of the reference fringe system.

The methodology of deciphering the phase is shown in Fig. 5. As one can see, the information about the phase shift in the whole range of z coordinate is obtained by interpolation or extrapolation of the value S at nodes. A very important question arising during the phase deciphering is how to determine the shifted value S in areas of interferogram in which due to the strong refraction of the probing radiation no interferometric fringes are observed. It especially concerns the plasma area near the target. The interpolation and the extrapolation of the shifted phase (for y_i = const) were carried out by means of the three degree splain function [8]. Over the range $z_1 < z < z_L$ (see Fig. 5) the shifted phase was interpolated by the splain function of the form

$$p_j(z) = \frac{1}{6h_j}[m_j(z_{j+1}-z)^3 + m_{j+1}(z-z_j)^3]$$

$$+\frac{1}{h_j}\left[\left(S_j - \frac{m_j h_j^2}{6}\right)(z_{j+1}-z) + \left(S_{j+1} - \frac{m_{i+1}h_j^2}{6}\right)(z-z_j)\right] \tag{4}$$

where $h_j = z_{j+1} - z_i$, $p_j(z) = y(z)$, $m_j = p''(z_j)$ and $j = 1, 2, 3 \ldots L$ (L – number of nodes).

For $z < z_L$, the following extrapolation was applied:

$$p(z) = S_1 - \frac{\frac{(z_2-z_1)m_2}{6} + (S_2 - S_1)}{(z_2-z_1)}(z-z_1), \tag{5}$$

however, for $z > z_L$, the value of S was extrapolated by the function of the form

$$p(z) = S_L + \frac{\frac{(z_L-z_{L-1})m_{L-1}}{6} + (S_L - S_{L-1})}{(z_L-z_{L-1})}(z-z_L). \tag{6}$$

In this way, by means of the procedure described above, the NETRAB program allows us to determine the phase distributions $S(y)$ for 512 cross-sections along coordinate z on the basis of the data taken with interferogram picture S. The phase distribution in the laser-produced plasma, as calculated with the use of the program block (Fig. 3) from the interferogram shown in Fig. 4**a**, is presented in Fig. 6.

Then the NETRAB program calculates on the basis of the Abel transformation (with the use of $S(y)$) the sought distributions of the function $f(r)$. The function $f(r)$ represents the electron density distribution. In order to obtain a correct reconstruction of the function $f(r)$ the Abel equation is resolved simultaneously using many numerical methods, both interpolation ones and those based on average-square

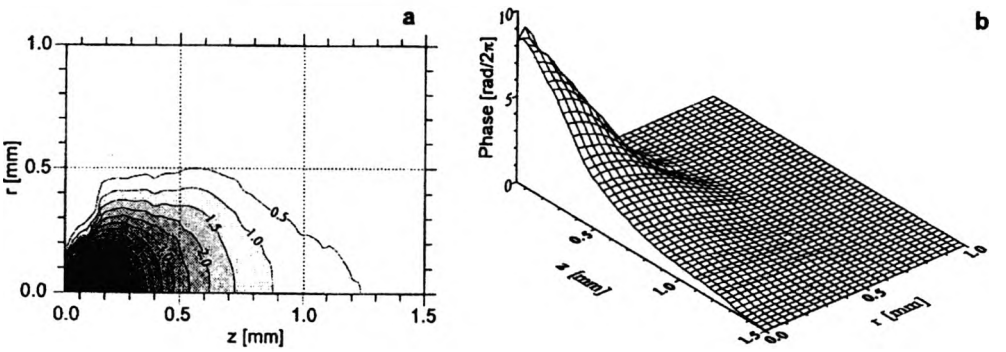

Fig. 6. Phase distribution calculated from the interferogram presented in Fig. 4: **a** – isodensitogram, **b** – phase profile.

approximation. In the case of investigations of the laser-produced plasma carried out at the Institute of Plasma Physics and Laser Microfusion the least-squares approximation method is applied with the use of the even Gegenbauer polynomials [4], [9]. The argumentation for selection of this method will be presented below.

Finally, the elaborated software (TRZYPE program, Fig. 3) enables us to obtain on the basis of the function $f(r)$ the information about the electron density distribution, linear electron density as well as about the total number of electrons in the plasma.

In the next part of this paper, selected numerical methods for resolving the Abel equation will be described. These methods were applied in the NETRAB procedure for determination of the electron density both in an axially symmetrical plasma and in a plasma stream of disturbed axial symmetry.

3. Determination of the electron density distribution in plasma by numerical methods

Measuring the phase shift S of an electromagnetic wave passing through a plasma one can obtain the average refractive index value along the probing direction, which makes it possible to determine the average electron concentration.

For some selected direction of plasma probing the relation between the refractive index and the electron density is [1]

$$S(x,y) = \frac{1}{\lambda}\int_A^B [1 - n(x,y)]\mathrm{d}s \cong 4.46 \times 10^{-14}\lambda \int_A^B n_e(x,y)\mathrm{d}s \tag{7}$$

where distance between A and B means a plazma size.

In the case of the optional plasma symmetry the interferometric measurements allow us to determine the electron density based on information about the phase shifting obtained from the probing of the plasma by means of a few beams simultaneously located at different angles (*i.e.*, the tomography method, [10]–[12]).

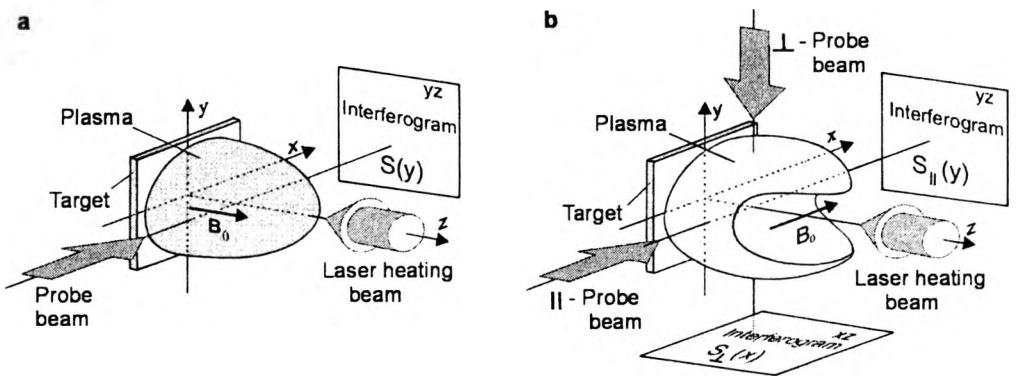

Fig. 7. Way of probing the axially symmetrical (**a**) and unsymmetrical plasma (**b**) in the interferometric measurement of the electron density distribution.

The number of probing directions depends on the degree of plasma symmetry. The number of these projections decreases with an increase of the plasma symmetry.

In the case of the laser-produced plasma located in an external magnetic field, which is generated inside a magnetic coil the number of diagnostic beams is limited by the coil construction. However, this plasma has some symmetry defined by the magnetic field distribution. In the case of experiment performed with axial geometry of the magnetic field the plasma is characterized by an axial symmetry because the magnetic lines are parallel to the direction of the main laser beam. For the axial symmetry of the plasma only one probing direction is just enough. As one can see in

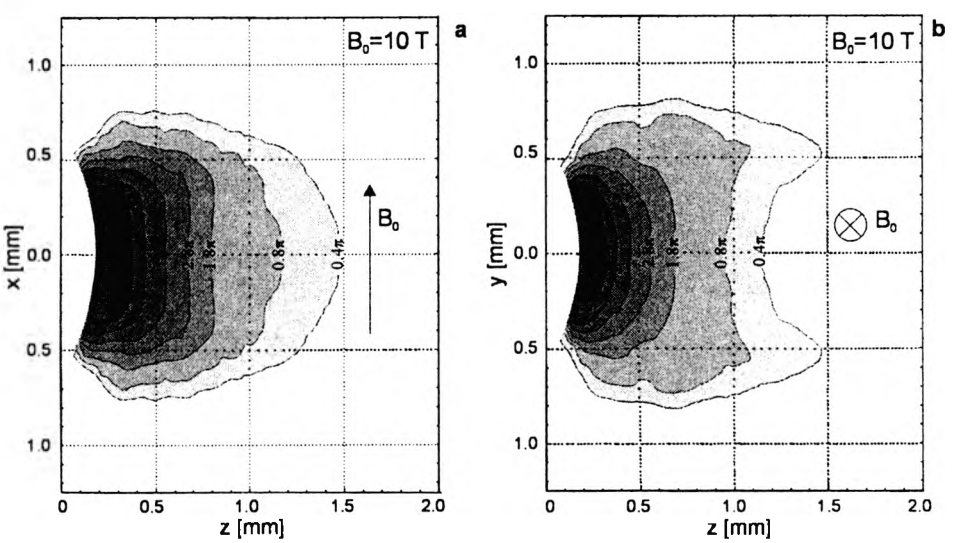

Fig. 8. Sample of the phase distributions which corresponds to the plasma of disturbed axial symmetry: **a** – registered perpendicularly, and **b** – parallel to the magnetic-field direction.

Fig. 7**a**, the diagnostic beam should be perpendicular to the symmetry axis of the plasma bubble.

Analyzing the symmetry of the plasma geometry in the transverse magnetic field it was assumed that the plasma stream was symmetrical with respect to the two mutually perpendicular planes, Fig. 7**b**. The *xz* plane is parallel to the direction of the magnetic field lines however the *yz* plane is perpendicular to this direction. For the purpose of reconstructing the electron density in this plasma there were selected two projections of the plasma probing which are illustrated in Fig. 7**b**. The above mentioned symmetry of the plasma was confirmed by the interferogram pictures registered perpendicularly (Fig. 8**a**) and parallel (Fig. 8**b**) to the magnetic field direction.

3.1. Determination of the electron density distribution in an axially symmetrical plasma

In the case of axial symmetry of the plasma the two-dimensional function $S(x, y)$ can be reduced to one-dimensional $S(y)$ and then the relation between the phase of the probing radiation and the electron concentration can be expressed as

$$S(y) = 8.92 \times 10^{-14} \lambda \int_{y}^{R} \frac{n_e(r) r}{\sqrt{r^2 - y^2}} \mathrm{d}r S(y) \tag{8}$$

where: $S(y)$ – the phase distribution of a probing beam in a selected cross section z of the plasma, [rad/2π], $n_e(r)$ – electron density distribution, [cm^{-3}], λ – wavelength of laser radiation, [cm].

The above equation has the form of the Abel integral equation [1], [4]

$$S(y) = 2 \int_{y}^{1} \frac{f(r) r}{\sqrt{r^2 - y^2}} \mathrm{d}r \tag{9}$$

where y and r are normalized spatial variables; $f(r)$ represents the distribution function

$$f(r) = 4.46 \times 10^{-14} \lambda R n_e(r). \tag{10}$$

The quantities y and r are defined in Fig. 9.

The solution of Eq. (9), known as the Abel integral inversion [1] (often named the Stielties integral equation), has the form

$$f(r) = -\frac{1}{\pi} \int_{r}^{1} \frac{S'(y)}{\sqrt{y^2 - r^2}} \mathrm{d}y \tag{11}$$

or

$$f(r) = -\frac{1}{\pi r} \frac{\mathrm{d}}{\mathrm{d}r} \int_{r}^{1} \frac{S(y) y}{\sqrt{y^2 - r^2}} \mathrm{d}y. \tag{12}$$

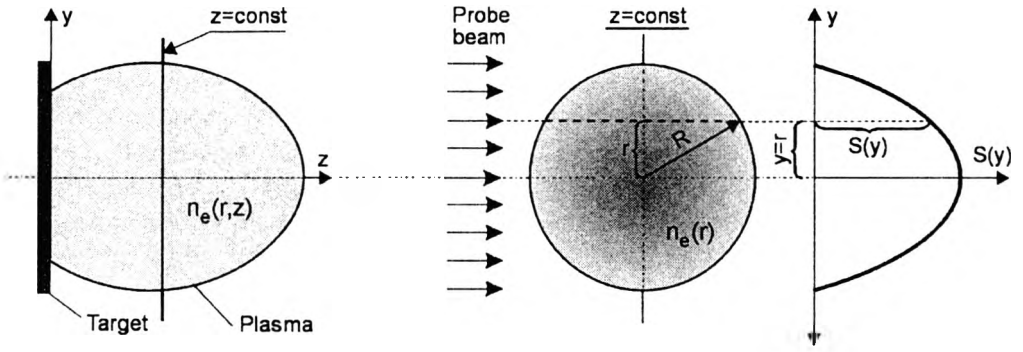

Fig. 9. Geometric interpretation of the Abel integral equation.

Thus, the question of obtaining the space distribution of electron density can be reduced to the determination of the function $f(r)$ on the basis of the above Abel transformations (11) or (12). The distribution function $f(r)$ can be determined only by means of selected numerical methods because the experimental function $S(y)$ is given in the form of measured values at many chosen points.

The interpolation and quadratic mean approximations are often used as a method of approximation, while the polynomials are employed as approximating functions because they are easily integrated.

When the measured values S_k at the points y_k ($k = 0, 1, ..., N$) are given, and the values f_k at the points r_k ($k = 0, 1, ..., N$) are searched for, then the Lagrange interpolation polynomial is used in the interpolation approximation [1]

$$S(y) = \sum_{k=0}^{n} \frac{(y-y_0)(y-y_1)\ldots(y-y_{k-1})(y-y_{k+1})\ldots(y-y_n)}{(y_k-y_0)(y_k-y_2)\ldots(y_k-y_{k-1})(y_k-y_{k+1})\ldots(y_k-y_n)} S_k. \tag{13}$$

In the quadratic mean approximation the sought function $f(r)$ is approximated by the linear combination of the orthogonal polynomials. The axial symmetry of the plasma makes it possible to use the even polynomials for the approximation.

Many authors have dealt with the solving of the Abel equation [9], [13]–[20]. The very important problem from the point of view of obtaining correct reconstruction of the space distribution of electron density in the plasma is selection of a proper numerical method for solving the Abel integral equation. An attempt was also made in this field by the authors of the present and other related papers [1], [2], [4], [21]. The results of those studies made it possible to choose appropriate numerical methods for the plasma under investigation. The fundamental criterion of the selection is the quality of reconstruction (by the selected methods) of suitable (for a given experiment) test functions which are connected with the electron density distribution.

Among the interpolation methods the most reliable and useful ones are methods which use the Lagrange interpolation polynomial of the degree $n = 0, 1$. Using interpolation polynomials of a degree higher than 1 was very ineffective.

When the function $f(r)$ is interpolated by a polynomial of $n = 0$, Eq. (9) is reduced to the expression

$$S_k = \frac{1}{N}\sum_{i=k}^{N-1} a_{k,i} f_i, \qquad k = 0, 1, \ldots, N-1, \tag{14}$$

from which, after transformations, the set of N equations is obtained, recurrent with respect to N unknowns of the value f_i

$$f_i = \frac{1}{a_{i,j}}\left(Ny_i - \sum_{k=i+1}^{N-1} a_{i,k} f_k\right), \qquad i = 0, 1, \ldots, N-1 \tag{15}$$

where

$$a_{i,k} = 2(\sqrt{(k+i)-i^2} - \sqrt{k^2 - i^2}), \qquad k \geq i. \tag{16}$$

The above way of determining of the distribution function $f(r)$ with the use of the Lagrange interpolation polynomial of zero degree is named the Mach–Schardin method [13], [14].

From among the group of methods based on the least-squares approximation there was selected the one which uses the even Gegenbauer polynomials [9].

In the case of this method the function $f(r)$ is approximated by the even polynomial of the form

$$f(r) = \sum_{i=1}^{k} A_l^{(k)} r^{2l}. \tag{17}$$

The degree of this polynomial $n = 2k$ cannot be too high (usually $n \ll N$ is assumed). On the left-hand side of the Abel equation (9) instead of the experimental function $S(y_i)$ we use its analytic approximation in the form

$$\bar{S}(y) = \sum_{j=0}^{k} B_j G_{2j}(y)\sqrt{1-y^2} \tag{18}$$

where $G_{2j}(y)$ are the Gegenbauer polynomials $C_{2l}^{p}(y)$ with the index $p = 3/2$ [9], and:

$$G_{2j}(y) = \sum_{n=0}^{j} \alpha_{n,j} y^{2n}, \tag{19}$$

$$\alpha_{n,j} = \left(-\frac{1}{2}\right)^{j-n} \frac{[2(j+n)+1]!!}{(2n)!(j-n)!}. \tag{20}$$

The coefficients B_j are obtained from the condition that the residual sum of squares is a minimum

$$R_k = \sum_{i=0}^{n} [S(y_i) - \bar{S}(y_i)]^2. \tag{21}$$

To this end there are applied the conditions of orthogonality of the Gegenbauer polynomials. We then obtain for B_j the expression

$$B_j = \frac{4j+3}{2(2j+1)(2j+2)} \int_{-1}^{1} S(y) G_{2j}(y) \sqrt{1-y^2}\, dy. \tag{22}$$

After substituting (17) in the Abel equation (9) with the left hand-part of $S(y)$, we obtain the expression for $A_l^{(k)}$

$$A_l^{(k)} = \sum_{j=0}^{k} \varepsilon_{l,j} B_j. \tag{23}$$

The matrix $\varepsilon_{i,j}$ is defined as follows:

$$\varepsilon_{0,0} = 1, \tag{24}$$

$$\varepsilon_{i,j} = \frac{\alpha_{j,j}}{\kappa_{j,j}} \quad \text{for} \quad j \geq 1, \tag{25}$$

$$\varepsilon_{j-1,j-1} = \frac{1}{\kappa_{j-1,j-1}} \left[\alpha_{j-1,j} - \sum_{n=j-l+1}^{j} \kappa_{j-1,n} \varepsilon_{n,j} \right] \quad \text{for} \quad 1 \leq l \leq j \tag{26}$$

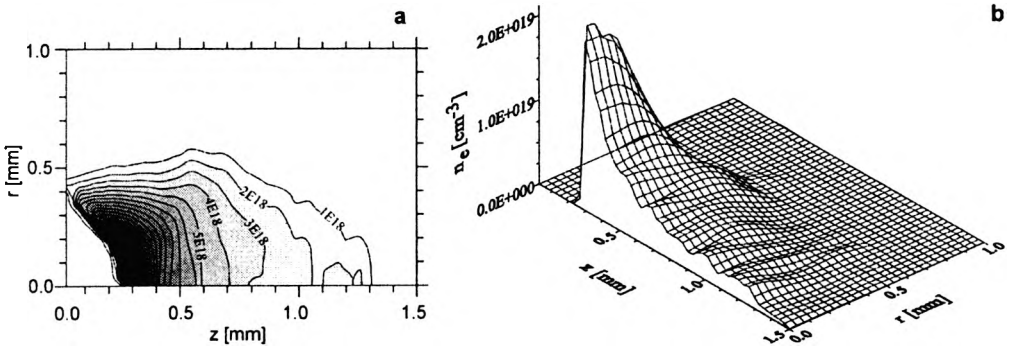

Fig. 10. Electron density distribution calculated on the basis of the shifted phase distribution presented in Fig. 6: **a** – isodensitogram, **b** – space profile.

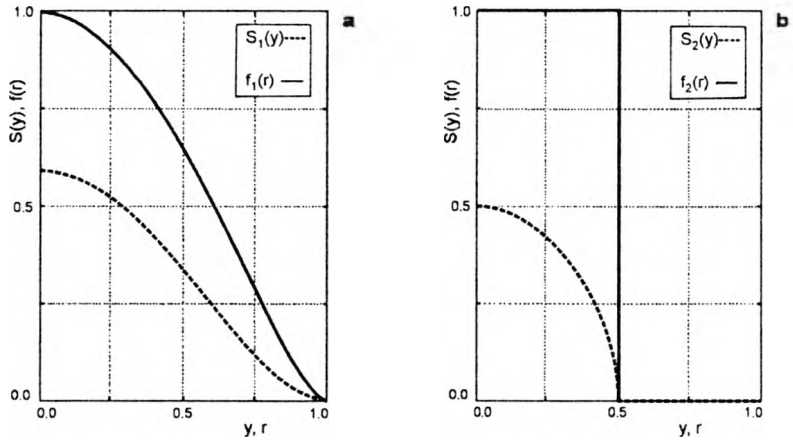

Fig. 11. Test functions: **a** – continuous, **b** – discontinuous.

where

$$\kappa_{i,k} = \sum_{l=k-i}^{k} \frac{(-1)^{l+i-k}}{2l+1} \begin{bmatrix} k \\ l \end{bmatrix} \begin{bmatrix} l \\ k-l \end{bmatrix} \quad \text{for} \quad k \geq 0,\ 1 \leq l \leq j. \tag{27}$$

The error of $f(r)$ can be estimated as follows:

$$\Delta f(r) = \left[\sum_{l=0}^{k} r_{2l} (\Delta A_l^{(k)})^2 \right]^{1/2} \tag{28}$$

where $\Delta A_l^{(k)}$ is the standard deviation of the coefficient defined by the expression

$$\Delta (A_l^{(k)})^2 = \sum_{i=l}^{k} \varepsilon_{i,j}^2 \left[\frac{4i+3}{2(2i+1)(2i+2)} \right] \frac{R_k}{N - n/2 - 1}. \tag{29}$$

After determination of the coefficients $\Delta A_l^{(k)}$ and the distribution function $f(r)$, the electron density distribution (see Fig. 10) was obtained on the basis of relation (10).

Both of the numerical methods were tested by means of the different kinds of the distribution functions $f(r)$ which are presented in Fig. 11. The first one is a continuous function (see, Fig. 11**a**) of the form

$$f_1(r) = \sqrt{(1 - r^2)^3}, \tag{30}$$

however, the second one is a discontinuous function (see, Fig. 11**b**) of the form

$$f_2(r) = \begin{cases} 1 & \text{for} \quad 0 \leq r \leq 0.5 \\ 0 & \text{for} \quad 0.5 < r \leq 1. \end{cases} \tag{31}$$

Based on the test functions $f(r)$ there were derived analytic formulas which describe the phase distribution function $S(y)$. This derivation was possible after integration of the Abel equation (9), and after substituting the function $f(r)$ in this equation.

The phase distribution function corresponding to equation (30) has the form

$$S_1(y) = \frac{3\pi}{8}(1-y^2)^2, \tag{32}$$

however, in the case of Eq. (31)

$$S_2(y) = \begin{cases} 2\sqrt{0.25-y^2} & \text{for} \quad 0 \le y \le 0.5 \\ 0 & \text{for} \quad 0.5 < y \le 1. \end{cases} \tag{33}$$

Then, using the values of $S_k(y)$ at the points y_k $(k = 0, 1, \ldots, N)$ the distribution function $f(r)$ was reconstructed by means of these numerical methods. A comparison of the results of the numerical calculation with the input data is given in Figs. 12, 13.

The following conclusions were drawn on the basis of a relatively simple analysis:

– As it is seen in Figs. 12**a** and 13**a**, the interpolation method (in spite of that it is numerically uncomplicated) correctly reconstructs the input distributions (Fig.11) in the whole range of y-coordinate for both of the test functions. However, the least-square approximation method is ineffective in the case of a very strong gradient or discontinuity of the distribution function $f(r)$ (see Fig.13**b**).

– The least-squares approximation method allows us to obtain more exact results in the case of continuous distributions (see Fig. 12**b**). Moreover, when the

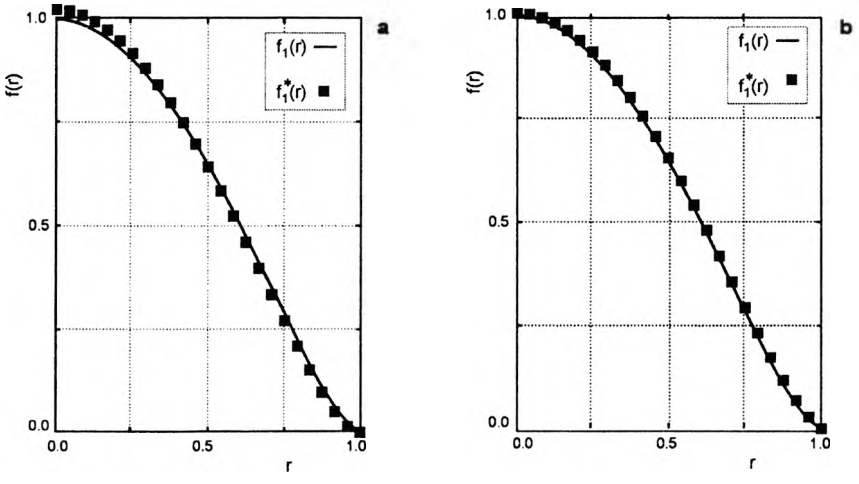

Fig. 12. Reconstruction of the continuous function by means of the Mach–Schardin interpolation method (**a**), the least-squares approximation method which uses the even Gegenbauer polynomials for the approximation (**b**).

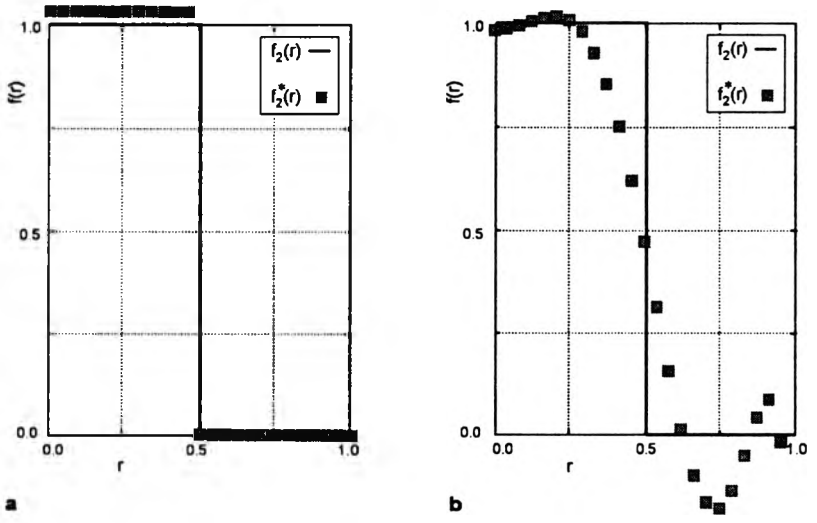

Fig. 13. Reconstruction of the discontinuous function by means of the Mach–Schardin interpolation method (**a**), the least-squares approximation method with the use of the even Gegenbauer polynomials for approximation (**b**).

plasma is not entirely axially symmetrical this numerical method automatically smoothes out and makes the input data symmetrical in relation to the assumed axis of symmetry. In the case of the interpolation method the smoothing procedure of the measurement data must be performed additionally before the numerical calculations are carried out.

The least-square approximation method which uses the even Gegenbauer polynomials was selected in order to prepare the NETRAB procedure because the plasma investigated (in an external magnetic field) did not reveal too strong gradients of the electron density.

3.2. Determination of the electron density distribution in the plasma with disturbed axial symmetry

When the plasma under investigation is considerably different from that of axially symmetrical it is indispensable to apply a tomographic interferometry. This is connected with the necessity of probing the plasma in a few directions simultaneously. The methods of determination of the electron density in an asymmetrical plasma, which are proposed in literature (*e.g.*, [12]), are based on expansion of the experimental function $S(x, y)$ and of the sought distribution $n_e(x, y)$ in a Fourier series. When using the cylindrical coordinates (ρ, Θ) (see Fig.14) the above distribution functions can be expressed as:

$$S(\rho, \Theta) = S_0(\rho) + \sum_{k=1}^{\infty} (S_{1k}(\rho)\cos k\Theta + S_{2k}(\rho)\sin k\Theta), \tag{34}$$

$$n_r(r, \Theta) = n_{e0}(r) + \sum_{k=1}^{\infty} (n_{e1k}(r)\cos k\Theta + n_{e2k}(r)\sin k\Theta) \tag{35}$$

where: ρ – the distance between the probing beam and the beginning of the coordinate system (Fig. 14), Θ – the angle between the normal to the probing beam and the x-axis direction.

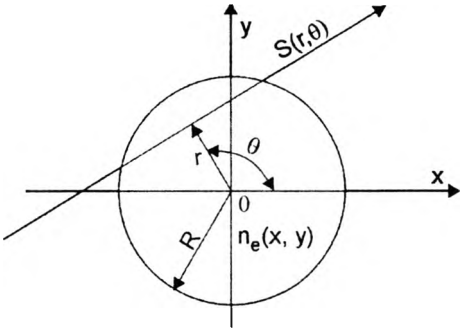

Fig. 14. Geometry of measurement in the case of polar coordinates.

After substituting the above series (34) and (35) in the Abel equation (8) and transformations we obtain the system of integral equations in the form:

$$S_0(\rho) = 8.92 \times 10^{-14}\lambda \int_{\rho}^{R} \frac{n_{e0}(r)r\mathrm{d}r}{\sqrt{r^2 - \rho^2}}, \tag{36}$$

$$S_{1,2k}(\rho) = 8.92 \times 10^{-14}\lambda \int_{\rho}^{R} \frac{n_{e1,2k}(r)r\mathrm{d}r}{\sqrt{r^2 - \rho^2}}. \tag{37}$$

Because the number of terms in the expansion of $S(\rho, \Theta)$ is dependnt on the number of projections, the number of probing directions in the plasma experiment is defined by the number of the first elements in the Fourier series. In our experiment (due to a limited access to the plasma located inside the magnetic coil), it was possible to probe the plasma only in two mutually perpendicular directions (see Fig. 7**b**). In the case of the measurement geometry considered the development $S(\rho, \Theta)$ reduces to the form

$$S(\rho, \Theta) = S_0(\rho) + S_{1,2}(\rho)\cos 2\Theta. \tag{38}$$

However, the sought function of the electron density distribution $n_e(r, \Theta)$ can be expressed as follows:

$$n_e(r, \Theta) = n_{e0}(r) + n_{e1,2}(r)\cos 2\Theta. \tag{39}$$

As it is seen, the distribution function $S(\rho, \Theta)$ is relatively simple and the second element of this development represents the disturbance of the axial symmetry which is connected with the first element.

The application of the method described above for reconstruction of the electron density in our experiment did not give correct results. Apart from the methods based on the expansion of the functions S and n_e in a Fourier series there was also applied the procedure described in [10]. In this procedure the axially symmetrical part of the plasma is represented by an arithmetic mean of the phase shifting for two mutually perpendicular projections, and the asymmetrical part is equal to half the difference between these phases. However, the testing shows that this method is useless, too. This method only enables us to obtain correct reconstruction of the electron density distribution in the case of very small disturbances of the plasma symmetry. Therefore, to reconstruct the spatial distribution of the electron density, we applied a methodology developed for the experiment under consideration [22]. Elaborating this methodology we took into account the fact that the plasma stream which we investigated, initially symmetrical, underwent deformation only in the front layer ($z > 0.4$ mm). Along its total length, the plasma stream kept approximately a circular cross-section, while the axial unsymmetrical part of the plasma was characterized by symmetry with respect to the xz and yz planes (see Fig. 8). This justifies the assumption that the distribution of n_e is superposition of two distributions: axially symmetrical and asymmetrical ones.

When the plasma is tested in two directions, parallel ($\parallel$) and perpendicular ($\perp$) to the direction of magnetic field lines, we obtain two phase distributions, $S_{\parallel}(y)$ and $S_{\perp}(x)$ for each cross-section parallel to the target surface (z = const, Fig. 7**b**).Then, we assumed that $S_{\parallel}(y)$ has two components

$$S_{\parallel}(y) = S_0(y) + S_1(y) \tag{40}$$

where: $S_0(y)$ corresponds to the part of the plasma having axial symmetry, while $S_1(y)$ corresponds to the asymmetrical part of the plasma.

Typical phase distributions of the functions $S_{\parallel}(y)$ and $S_{\perp}(x)$ as well as $S_0(y)$ and $S_1(y)$ determined on the basis of $S_{\parallel}(y)$ are presented in Fig. 15. According to Fig. 15, the values $S_0(y)$ of the components are correctly determined on the axis ($y = 0$) and at the point $y = R$ on the plasma edge. On the axis: $S_0(0) = S_{\parallel}(0)$, while on the plasma border: $S_0(R) = S_{\parallel}(R)$. In the range from $y = 0$ to $y = R$ the function $S_0(y)$ was approximated by the expression

$$S_0(y) = \frac{S_{\parallel}(y) + S_m(y)}{2}, \tag{41}$$

assuming the linear character of the function $S_m(y)$

$$S_m(y) = -\frac{S_{\parallel}(0)}{R} y + S_{\parallel}(0). \tag{42}$$

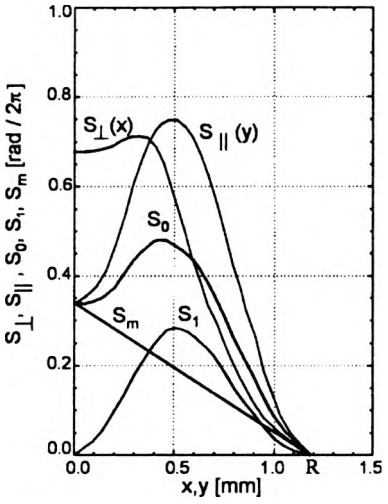

Fig. 15. Symmetrical $S_0(y)$ and unsymmetrical $S_1(y)$ functions obtained on the basis of the phase distribution functions $S_{\|}(y)$ and $S_{\perp}(y)$.

After obtaining the symmetrical component, the unsymmetrical component can be expressed as follows:

$$S_1(y) = S_{\|}(y) - S_0(y). \tag{43}$$

Because the plasma stream under investigation kept approximately a circular cross -section (along its total length) it was possible to determine the distributions $n_{e0}(r)$ and $n_{e1}(r)$ based on the information about the symmetrical function – $S_0(y)$, and the unsymmetrical one – $S_1(y)$ and using the Abel equation (8). According to Eq. (12), the expressions which describe the distributions $n_{e0}(r)$ and $n_{e1}(r)$ take the form:

$$n_{e0}(r) = \frac{0.22 \times 10^{14}}{\pi \lambda r R} \frac{\mathrm{d}}{\mathrm{d}r} \int_r^1 \frac{S_0(y) y}{\sqrt{y^2 - r^2}} \mathrm{d}r, \tag{44}$$

$$n_{e1}(r) = \frac{0.22 \times 10^{14}}{\pi \lambda r R} \frac{\mathrm{d}}{\mathrm{d}r} \int_r^1 \frac{S_1(y) y}{\sqrt{y^2 - r^2}} \mathrm{d}r. \tag{45}$$

In order to express the electron density distribution in polar coordinates (r, θ), the following empirical formula was used:

$$n_e(r, \theta) = A n_{e0}(r) + B n_{e1}(r)(1 - \cos 2\theta) \tag{46}$$

where A and B are the matching coefficients.

The distribution $n_e(r, \theta)$ obtained with this method was verified by numerical calculation of corresponding distributions $S_{\|}^*(y)$ and $S_{\perp}^*(y)$ (on the basis of $n_e(r, \theta)$)

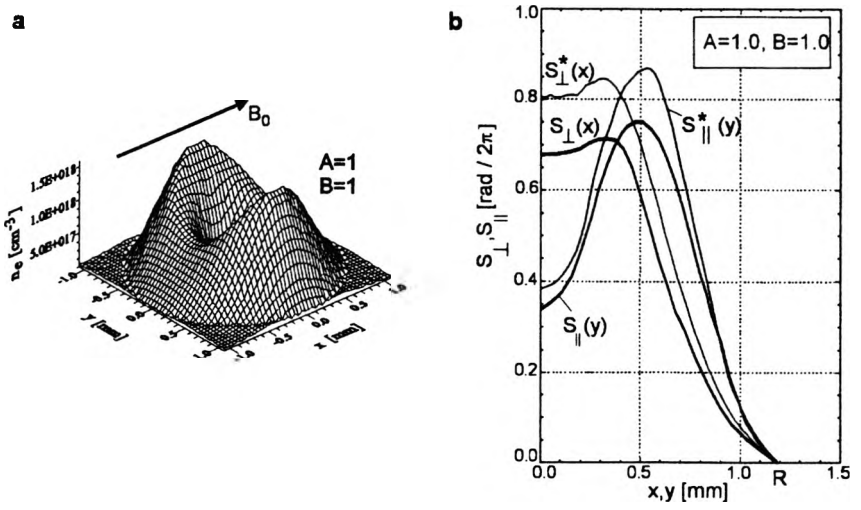

Fig. 16. Illustration of the methodology used for reconstruction of the electron density distribution: **a** – space distribution of the electron density calculated for the following values of the coefficients: $A = 1$ and $B = 1$, **b** – comparison of the experimental phase distributions ($S_{||}(y)$ and $S_\perp(x)$) with the numerical modeled phase distributions $S_{||}^*(y)$ and $S_\perp^*(x)$.

and their comparison with the experimental distributions $S_{||}$ and $S_\perp$. The coefficient A was taken such that we could recover precisely the distribution $S_\perp$ near the axis of symmetry that was in the region where the asymmetric part of the plasma stream did not interfere, whereas the coefficient B was to provide recovery of the distribution $S_{||}$ and the remaining part of the distribution $S_\perp$.

In order to determine the electron density in the unsymmetrical plasma in a transverse magnetic field the TOMOGRAF program block was developed. In the first step, the TOMOGRAF enables determination the distributions S_0 and S_1 on the basis of phase distributions $S_\perp(x)$ and $S_{||}(y)$. To determine these phase distributions the NETRAB program (described in Section 3) is applied. Then the electron density distribution in polar coordinates (r, θ) is calculated using empirical formula (46).

The coefficients A and B in the solution (46) were adjusted by a numerical modeling. This modeling is continued up to the moment when the phase distributions $(S_\perp^*, S_{||}^*)$ become the same as the experimental ones ($S_\perp$ and $S_{||}$). The methodology of determination of the coefficients A and B is illustrated in Figs. 16–18, respectively. In the first stage, the coefficient A is matched, which is responsible for reconstruction of the phase distribution ($S_{||}$) near the axis of symmetry. For this reason at the beginning of the calculation, assuming $A = 1$ and $B = 1$, the electron density distribution is determined by means of the TOMOGRAF procedure, Fig. 16**a**. Then on the basis of the distribution $n_e(r, \theta)$ there are calculated the distributions $S_\perp^*$ and $S_{||}^*$ and these distributions are compared with the experimental ones $S_\perp$ and $S_{||}$ (see Fig. 16**b**). Then, changing the value of the coefficient A (for B = const) further calculations are carried out up to the moment the value of $S_{||}^*(0)$ is equal to the experimental value of

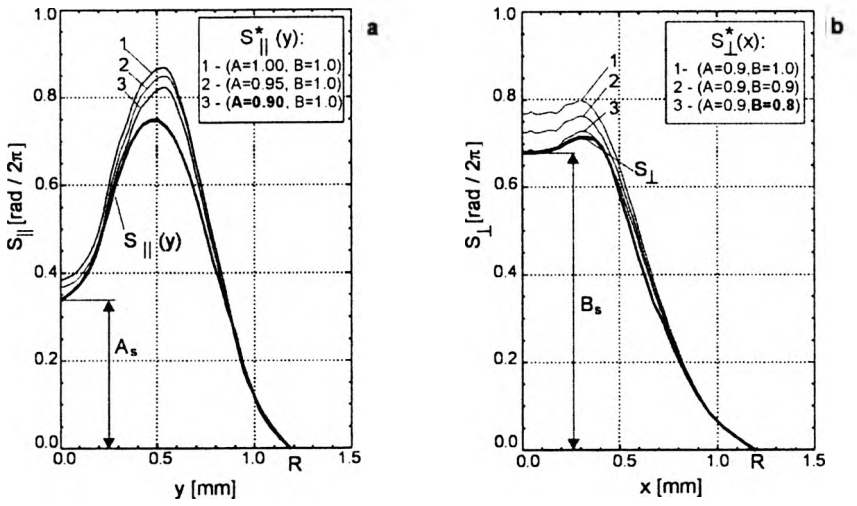

Fig. 17. Illustration of the methodology used for reconstruction of the electron density distribution: **a** – matching of the coefficient A, and **b** – matching of the coefficient B.

$S_{\|}(0)$ (see the A_s value in Fig. 17**a**). The matching of the coefficient A is shown in Fig. 17**a**. After determining the optimal value of coefficient A the coefficient B is matched, Fig. 17**b**. As it follows from the calculation the matching of the optimal value of B enables us not only to recover precisely the $S_{\perp}^{*}$ near the symmetry axis (see the B_s value in Fig. 17**b**) but also allows us to reconstruct correctly both of the phase distributions ($S_{\|}^{*}$ and $S_{\perp}^{*}$) in the whole range of the x, y coordinates. The electron

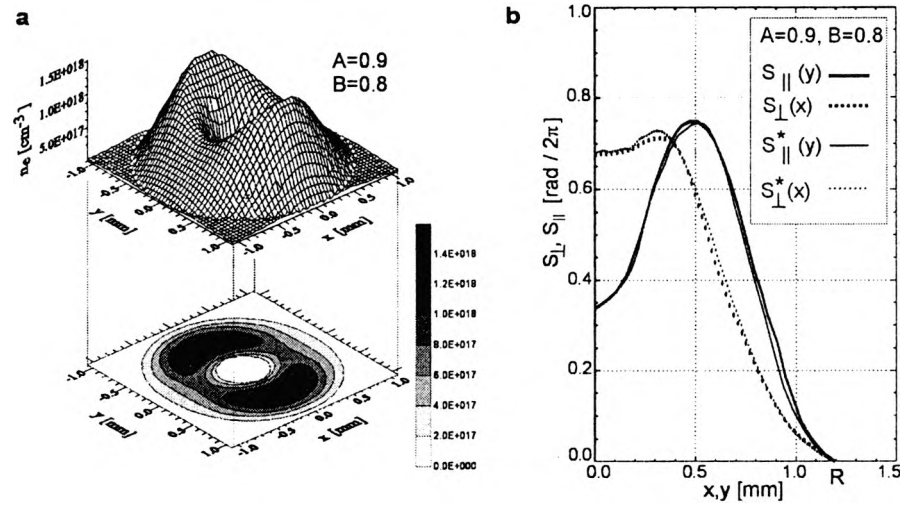

Fig. 18. Illustration of the methodology used for reconstruction of the electron density distribution: **a** – the electron density distribution calculated for the optimal values of coefficients A and B, **b** – comparison of the experimental and numerical phase distributions.

density distribution obtained and the comparison of the experimental phase distributions with the numerically modelled distributions of phase after matching the coefficients A and B are presented in Fig. 18.

Then the TOMOGRAF program calculates the electron density $n_e(r, \theta)$ in 512 cross-sections (parallel to target surface) of the plasma bubble. Moreover, the TOMOGRAF procedure enables us to illustrate graphically the electron density in the optionally selected plane of the plasma bubble.

A relatively good conformity of the experimental phase distribution $(S_\perp(x), S_\parallel(y))$ and the optimal phase distribution $(S_\perp^*, S_\parallel^*)$ which was obtained by the TOMOGRAF procedure justifies the assumption about the plasma symmetry with respect to the two planes. It enables us to realize the interferometric measurements of the laser plasma in a transverse magnetic field by means of the two projections only and to apply relatively simple numerical procedures for reconstruction of the plasma electron density.

4. Interferometric investigations of the laser-produced plasma in strong external magnetic field

In this section, some results of the interferometric investigations of the laser-produced plasma in a strong external magnetic field of 5 T up to 15 T in induction and a force-lines geometry both parallel and transverse to the laser heating beam direction are presented. Detailed results of these investigations are available in papers [22]–[30].

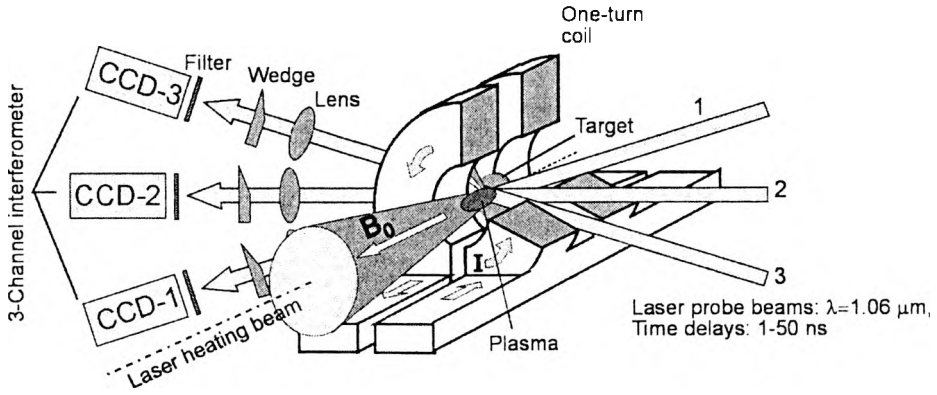

Fig. 19. Schematic drawing of the location of the interferometer in the experiment.

These studies were carried out for a plasma generated from a flat teflon target irradiated with a neodymium laser beam of energy 5–10 J and pulse duration of about 1 ns (FWHM). The interferometric system was illuminated with a part of the beam generated by the same laser. Locations of the interferometer in the experiments for both geometries of the magnetic field are shown in Figs. 19 and 20.

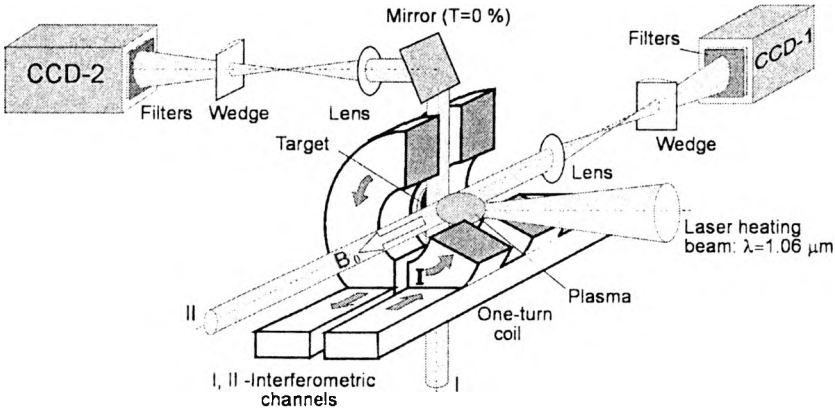

Fig. 20. Location of the two-channel interferometer in the experiment.

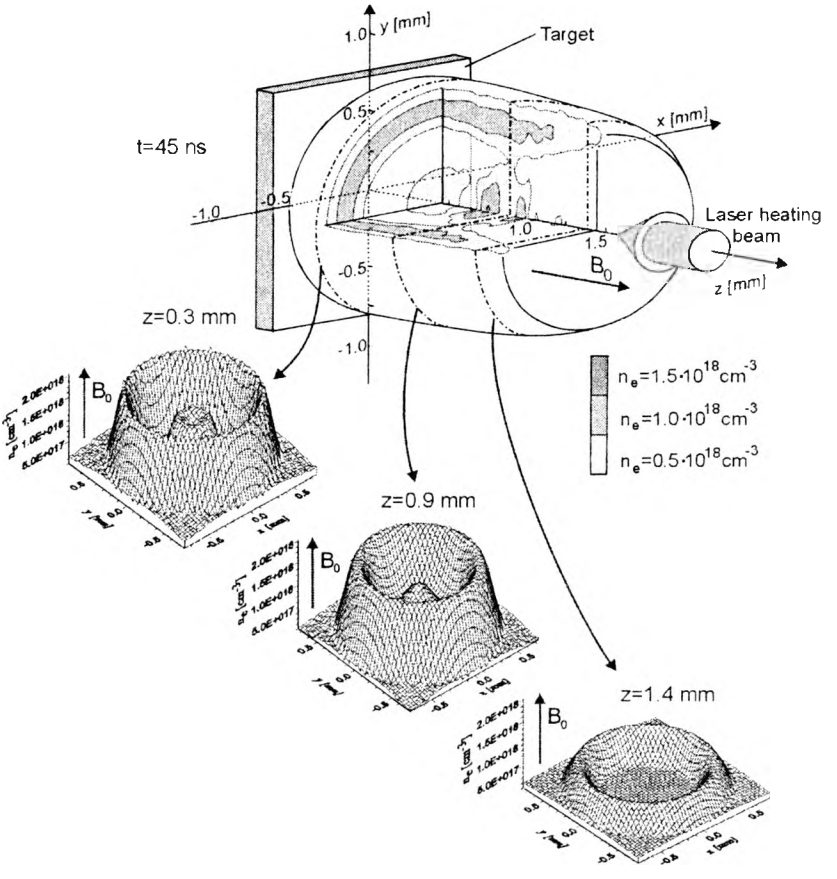

Fig. 21. Electron density distribution of the plasma stream obtained for the angular plasma expansion in the presence of the axial magnetic field of 17 T in induction.

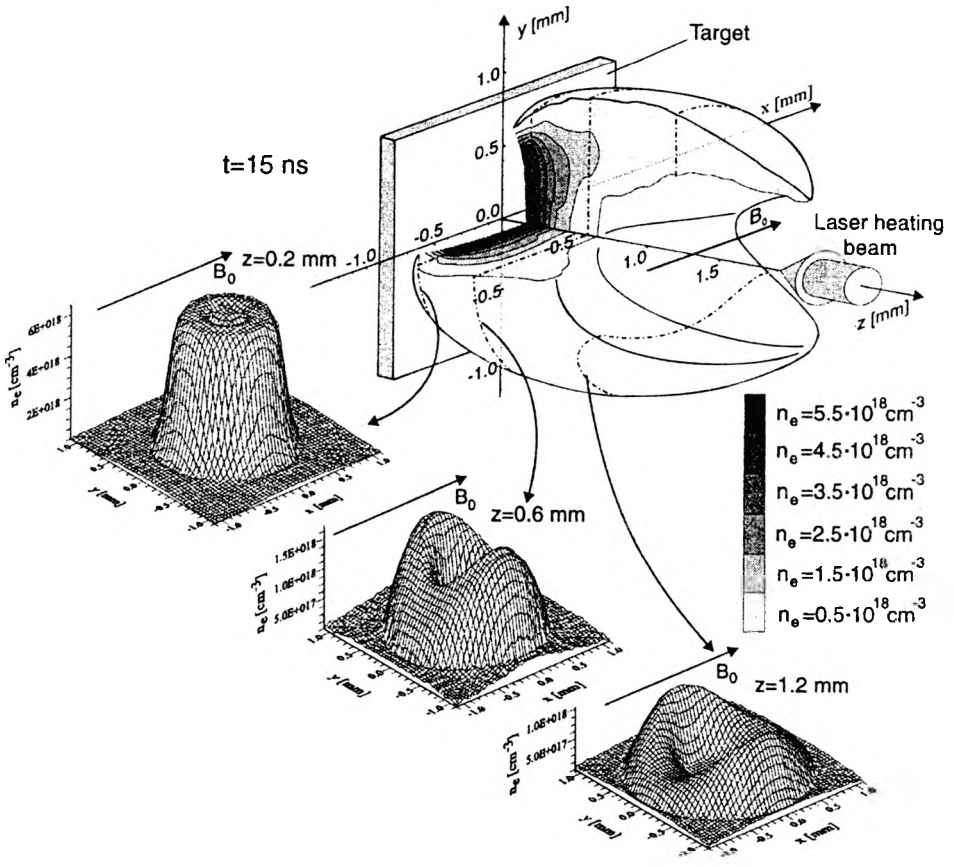

Fig. 22. Spatial distribution of the electron density in the diamagnetic cavity created in the presence of the transverse magnetic field of 10 T in induction.

In the case of a parallel magnetic field, two kinds of plasma expansion were observed, *i.e.*, the angular and axial one, related to the target illumination conditions. The more interesting angular plasma expansion is characterized by the development of a specific paraboloid-shaped plasma configuration with the apex situated near the target. In the final stage of its evolution, the paraboloid is transformed into a tube of about 1 mm in length with the radius proportional to $B_0^{2/3}$ [23], [25], [26]. This shape of the plasma stream is shown in Fig. 21.

In the second case, the interferometric measurements have shown that a transverse magnetic field induces an asymmetry of the plasma which is distinctly visible in the interferograms registered in two mutually perpendicular directions. The plasma electron density distributions in a plasma stream of the disturbed axial symmetry, reconstructed by the methodology prepared for this experiment, are presented in Fig. 22. It has been proved it is the Rayleigh–Taylor instability [22], [29] that is responsible for the disturbance of axial symmetry of the plasma.

5. Conclusion

The results of the interferometric measurement of the laser-produced plasma in an external magnetic field show that the modern interferometric system used is a very complex diagnostic tool for the plasma. The plasma investigated imposes high requirements which are connected with its external parameters such as high dynamics, very short life-time, high electron density near the target and relatively small dimensions. Therefore, the investigation of the high-temperature plasma stream requires both application of the multi-frame automated interferometric systems for registration of interferograms and professional software for their fast analysis.

The interferometric system presented here is completely original, and no equivalent of the system can be found in articles describing the investigation of the laser plasma by means of interferometry. For this reason, the results presented by the authors and related to the interferometric studies of the laser plasma (and especially those related to the plasma confined by a strong magnetic field) constitute an important and original achievement of the authors, which fact is confirmed by numerous publications.

References

[1] KASPERCZUK A., PADUCH M., POKORA L., WERESZCZYŃSKI Z., J. Techn. Phys. **19** (1978), 137.
[2] PISARCZYK T., ARENDZIKOWSKI R., PARYS P., PATRON Z., Laser Part. Beams **12** (1994), 549.
[3] KASPERCZUK A., MAKOWSKI J. PADUCH M., *et al.*, Proc. SPIE **2202** (1993), 449.
[4] PISARCZYK T., RUPASOV A. A., SARKISOV G. S., SHIKANOV A. S., J. Sov. Laser Res. **11** (1990), 1.
[5] TAKEDA M., INA H., KOBAYASHI S., J. Opt. Soc. Am. **72** (1982), 156.
[6] NOUGENT K. A., Appl. Opt. **24** (1985), 3101.
[7] KALAL M., Czech. J. Phys. **41** (1991), 743.
[8] VOLKOV E., *Metody obliczeniowe*, (in Polish), [Ed.] Nauka, Moscow 1982.
[9] GORENFLO R., Report IPP/6/19, 1964 Institut für Plasma Physik, Garching, Germany.
[10] GORBUNOV E. P., DNESTROVSKIJ YU. N., KOCTOMAROV D. P., J. Tech. Phys. (in Russian), **38** (1968), 812.
[11] LAPWORTH K. G., ALLNUT L. A., J. Phys. E (London). Sci. Instrum., **10** (1977), 733.
[12] PIKALOV V. V., MELNIKOVA T. S., *Niskotemperaturnaya plazma*, t. 13, *Tomografiya plazmy*, (in Russian), [Ed.] Nauka, Sibirskaya Izd. Firma RAN, Novosibirsk 1995.
[13] PEARCE W. J., [In]: Proc. Conf. *Extremely High Temperature*, Boston, Massachussets, March 18–19, Wiley, New York 1958, pp. 123–124.
[14] LADENBURG W., LEWIS W., PHEASE R. N., TAYLOR H. S., *Physical Measurement in Gas Dynamics and Combustion*, Vol. 9, [In]: *High Speed Aerodynamics and Jet Propulsion*, T. von Karman *et al.* [Eds.], Oxford Univ. Press, 1955.
[15] BOCKASTEN K., J. Opt. Soc. Am. **51** (1961), 943.
[16] FLEURIER C., CHAPELLE J., Comput. Phys. Commun. **7** (1974), 200.
[17] SWEENEY D. W., ATWOOD D. T., COLEMAN L. W., Appl. Opt. **15** (1976), 1126.
[18] FAN L. S., SQUIRE W., Comput. Phys. Commun. **10** (1975), 98.
[19] ZAKHARENKOV YU. A., KROKHIN O. N., SKLIZKOV G. V., SHIKANOV A. S., Sov. J. Quantum Electron. **6** (1976), 571.
[20] SADOWSKI M., UGNIEWSKI S., J. Tech. Phys. **17** (1976), 365.

[21] KASPERCZUK A., PADUCH M., PISARCZYK T., *et al.*, *Numerical methods of treatment of the interferometric picture of a plasma with the use of the Abel integral equation*, (in Polish), Report IPPLM-1977, Institute of Plasma Physics and Laser Microfusion, Warszawa, Poland.
[22] PISARCZYK T., KASPERCZUK A., Laser Part. Beams **17** (1999), 313.
[23] PISARCZYK T., BRYUNETKIN B. A., FAENOV A. YA., *et al.*, Phys. Scr. **50** (1994), 72.
[24] KASPERCZUK A., PISARCZYK T., Phys. Scr. **53** (1996), 503.
[25] KASPERCZUK A., MIKLASZEWSKI R., PISARCZYK T., Phys. Scr. **54** (1996), 636.
[26] KASPERCZUK A., PISARCZYK T., ZIELIŃSKA E., J. Mosc. Phys. Soc. **5** (1996), 237.
[27] DYAKIN V. M., FAENOV A. YA., MAGUNOV A. I., *et al.*, Phys. Rev., A **54** (1996), 3971.
[28] DYAKIN V. M., MAGUNOV A. I., PIKUZ T. A., *et al.*, Sov. J. Quantum Electron. **27** (1997), 1017.
[29] KASPERCZUK A., PISARCZYK T., ZAKHAROV YU. P., Laser Part. Beams **7** (1999), 537.
[30] PISARCZYK T., KASPERCZUK A., MIKLASZEWSKI R., ZAKHAROV YU. P., Opt. Appl. **30** (2000), 41.

Received December 7, 2000
in revised form April 17, 2001